Damage detection based on stiffness identification in time domain for poly-linear hysteresis using sparse modeling

Nabeshima, Kunihiko

(Citation)
Earthquake Engineering & Structural Dynamics,52(12):3533-3550

(Issue Date)
2023-10-10

(Resource Type)
journal article

(Version)
Accepted Manuscript

(URL)
https://hdl.handle.net/20.500.14094/0100483144

Damage detection based on stiffness identification in time domain for poly-linear hysteresis using sparse modeling

Kunihiko Nabeshima [1]

[1] Dept. of Architecture, Grad. School of Eng., Kobe Univ., Rokkodai-cho, Nada-ku, Kobe, Japan

The physical parameter identification of the dynamic mechanical model, such as stiffness identification, provides some valuable information for detecting post-earthquake damage to building structures. During an earthquake, tracking changes in stiffness on the skeleton curve can be effective. It would also be helpful as an approximate evaluation if the method could be applied to structures with arbitrary poly-linear hysteresis characteristics. However, previous research has not identified any poly-linear hysteresis characteristics in a unified formulation. This paper proposes a new stiffness identification method in the time domain for building structures with any poly-linear hysteresis characteristics using sparse modeling. The validity of the proposed method was investigated through numerical simulations and a full-scale shaking table test.

KEYWORDS

damage detection, stiffness identification, nonlinear structure, poly-linear hysteresis, sparse modeling, time-domain, full-scale shaking table test

INTRODUCTION

Structural health monitoring (SHM) consists of several key roles, such as checking the consistency of seismic performance between the structural design phase and post-construction, assessing the functionality of buildings and business continuity after an earthquake and the necessity of seismic retrofitting, and checking the retrofit performance and aging deterioration. Mainly, SHM that focuses on detecting damage during earthquakes is classified into four stages according to the damage evaluation level[1)]: an evaluation of the presence, source, degree of damage, and residual seismic performance. When a visual inspection is used to conduct these evaluations, the accuracy of the assessment depends highly on the constraints of the inspection place and the skills of the person conducting it, which can be a severe problem. As a result, the dynamic characteristics evaluation techniques based on vibration measurement (e.g., system identification) are widely used as fundamental techniques for supporting damage detection.

System identification can be broadly categorized into two types: nonparametric and parametric. The former is a method in which the model characteristics are evaluated directly based on measurement data without first defining the model. For instance, the transfer function is numerically estimated from measurement data or the cross-spectrum method[2)], and no parameters are involved in the identification process. The latter is a method in which the mathematical or physical model is previously and explicitly specified, and the model parameters are identified. Parametric identification methods include identification methods based on the Auto-Regressive eXogenous (ARX) model[3)] and shear-type vibration models. It is important to clarify the physical meanings of the evaluation values in damage assessment. Thus, parametric identification that makes it easier to clarify them is often adopted. For example, in parametric identification based on physical models (e.g., shear-type vibration models), modal parameters (e.g., natural frequencies, mode shapes, and mode damping ratios), and physical parameters (e.g., stiffness and damping coefficient) are the primary identification targets. These are known as the modal parameter identification[4-9)] and physical parameter identification[10-13)], respectively. Modal parameter identification is suitable for evaluating the global vibration characteristics of building structures and determining the presence of damage. However, the physical identification would be more effective for evaluating the source or degree of damage because a minor degree of damage at the member (e.g., column and beam) only slightly influences the modal vibration characteristics[14,15)]. On the other hand, considering that dynamic characteristics can change dramatically in a short time during an earthquake, coupled with the effects of nonlinearization, it is preferable to use a time-domain identification method to capture such transient changes in dynamic characteristics. If the variation in physical parameters of the building model can be evaluated during the earthquake, the investigation of the variation pattern can be useful for SHM.

Previous research has broadly classified time-domain physical parameter identification considering the nonlinear characteristics of structures into two methods: an identification method based on a sequential linear approximation[16-20)] and a direct identification method based on a nonlinear model[21-31)]. The former method has the advantage of being relatively simple and easy to implement. However, the degree and type of nonlinearity, and the resolution of the time domain, significantly impact its accuracy and reliability. In contrast, the latter method deals with nonlinear characteristics directly. It provides model-specific identification results, but its applicability is limited to bi-linear

models and Bouc-Wen models[21], and so on, and its generality is often an issue. That is because the direct formulation of inverse problems based on the kinematic equations involves a mathematical limit, multimodality of the objective function makes it difficult to search globally optimum parameters, and so on. Detecting stiffness change points (nonlinearization) on the skeleton curve in the time domain would significantly aid in detecting structure building damage. In this regard, it would be helpful as an approximate evaluation method if a method applicable to any poly-linear hysteresis characteristics (e.g., bi-linear and tri-linear types) is developed. However, because of the abovementioned difficulties, it is currently difficult to identify parameters in a unified method for arbitrary poly-linear hysteresis characteristics.

On the other hand, the identification methods for nonlinear dynamic systems focusing on sparse modeling[32-35] have been developed recently. Sparse modeling is a methodology for finding sparse solutions to regression problems in which many components of the solution vector are sparse (zero). It represents data from a few key pieces of information. Sparse modeling is effective in analyzing factors from results and is used in various research fields, such as image and signal processing, because of its features. Sparse modeling is expected to have various advantages, including improving the robustness of solutions to noise and solving under-determined equations. However, a system of basis functions (e.g., trigonometric functions, wavelet functions, and impulse responses) composing the data to be regressed (e.g., burden force in structural element) must be determined in advance. Since the regression target is represented by a linear combination of these basis functions, the identification accuracy and applicability depend on the assumption of the basis function system. In the case of targeting energy dissipation devices (e.g., members in passive control and seismic isolation buildings) that are standardized and quality-controlled in the mechanism, the constitutive law of the model is relatively definite. Therefore, selecting the candidate basis functions can be easier based on the damper characteristics[35]. However, selecting a basis function system is not easy because the building exhibits complex nonlinearity (e.g., stiffness deterioration and strength deterioration) in the case of seismic building structures. In addition, the adjustment of the hyperparameters, such as the regularization coefficients, often requires much effort.

This research focuses on the following points and develops a new stiffness identification method in the time domain (hereinafter, the "proposed method") that employs sparse modeling.

(1) Any poly-linear hysteresis characteristics can be identified in a unified process.
(2) No need to select the basis function system that composes the regression-target data.
(3) Robust to noise and few intervening hyperparameters

The first and second numbered bullet points are the primary features and advantages of the proposed method over previous methods. Introducing sparse modeling to realize the first point is also a feature of this research. The validity of the proposed method is discussed through numerical simulations and the full-scale shaking table test.

IDENTIFICATION THEORY OF PHYSICAL PARAMETERS IN TIME DOMAIN

A dynamic mechanical model used for the identification is shown in Fig. 1. In Fig. 1, $f(t), k(t)$ and c are the dynamic force, stiffness, and viscous damping coefficient, respectively, and the stiffness element is assumed to exhibit any nonlinear hysteresis characteristics. The stiffness and damping elements are assumed to be connected in parallel. The assumption that c is constant can be an issue of the proposed method. This method requires modeling the damping force in the time domain. Including the problem of dependency degree on frequencies, what kind of damping model is appropriate for elastoplastic behavior is still discussed as a topic and a complicated issue to research. In this paper, the simplest damping model is used to investigate the fundamental behavior of the proposed method.

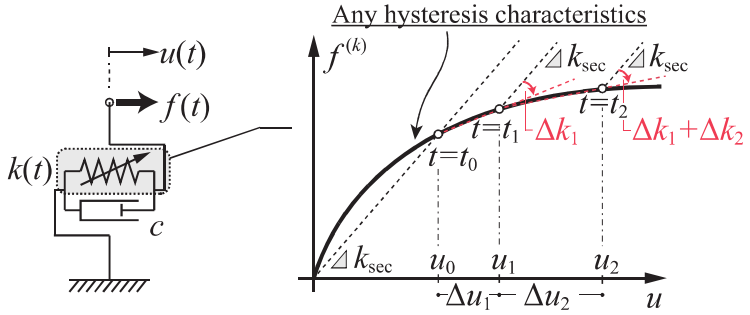

Figure 1 Dynamic mechanical model assumed for the identification

As shown in Fig.1, the force equilibrium in the dynamical model at a specific time t_0 can be denoted by

$$f(t_0) = f^{(k)}(t_0) + f^{(c)}(t_0) = k_{\text{sec}} u(t_0) + c\dot{u}(t_0) \tag{1}$$

where $f^{(k)}$ and $f^{(c)}$ are the restoring and damping forces, respectively. k_{sec} in Eq. (1) and Fig. 1 denotes the secant stiffness evaluated from the restoring force and deformation at a specific time t_0. As illustrated in Fig. 1, if the tangent stiffness at $t_n = t_0 + n\Delta t$ (Δt: time increment) is expressed approximately by Eq. (2), the restoring force $f^{(k)}(t_n)$ can be described by Eq. (3). Eq. (2) implies that any hysteresis characteristics are evaluated as poly-linear characteristics.

$$k(t_n) = k(t_0 + n\Delta t) = k_{\text{sec}} + \sum_{i=1}^{n} \Delta k_i \tag{2}$$

$$\begin{aligned} f^{(k)}(t_n) &= f^{(k)}(t_0 + n\Delta t) \\ &= k_{\text{sec}} u_0 + (k_{\text{sec}} + \Delta k_1)\Delta u_1 + (k_{\text{sec}} + \Delta k_1 + \Delta k_2)\Delta u_2 + \cdots + \left\{ k_{\text{sec}} + \sum_{i=1}^{n} \Delta k_i \right\} \Delta u_n \\ &= k_{\text{sec}} \left(\sum_{i=0}^{n} \Delta u_i \right) + \Delta k_1 \left(\sum_{i=1}^{n} \Delta u_i \right) + \Delta k_2 \left(\sum_{i=2}^{n} \Delta u_i \right) + \cdots + \Delta k_n \Delta u_n \end{aligned} \tag{3}$$

where Δk_i denotes the amount of stiffness variation that occurs during each discrete time, $u_i = u(t_0 + i\Delta t)$, and Δu_i ($= u_i - u_{i-1}$, $\Delta u_0 \equiv u_0$) is the deformation increment between discrete times. The following linear regression problem is derived from the force equilibrium equations up to n-discrete time based on Eqs. (1)–(3). The variable (t) will be omitted in the following formulations unless otherwise noted.

$$\mathbf{f} = \mathbf{A}\mathbf{p} \tag{4}$$

where,

$$\mathbf{f} = \begin{Bmatrix} f_0 \\ f_1 \\ f_2 \\ \vdots \\ f_n \end{Bmatrix} \in \mathbb{R}^{n+1},\ \mathbf{A} = [\mathbf{a_1}, \mathbf{a_2} \cdots \mathbf{a_{n+2}}] = \begin{bmatrix} u_0 & 0 & 0 & \cdots & 0 & \dot{u}_0 \\ u_1 & \Delta u_1 & 0 & \cdots & 0 & \dot{u}_1 \\ u_2 & \Delta u_1 + \Delta u_2 & \Delta u_2 & \cdots & 0 & \dot{u}_2 \\ u_3 & \sum_{i=1}^{3} \Delta u_i & \Delta u_2 + \Delta u_3 & \cdots & 0 & \dot{u}_3 \\ \vdots & \vdots & \vdots & \ddots & \vdots & \vdots \\ u_n & \sum_{i=1}^{n} \Delta u_i & \sum_{i=2}^{n} \Delta u_i & \cdots & \Delta u_n & \dot{u}_n \end{bmatrix} \in \mathbb{R}^{(n+1)\times(n+2)},\ \mathbf{p} = \begin{Bmatrix} k_{\text{sec}} \\ \Delta k_1 \\ \Delta k_2 \\ \vdots \\ \Delta k_n \\ c \end{Bmatrix} \in \mathbb{R}^{n+2} \tag{5}–(7)$$

The features and advantages of this formulation are summarized as follows. Previous research (as seen in an example in reference[35]) requires the selection and assumption of a basis function system (corresponding to the column basis of matrix **A** in Eq. (4)) for a given nonlinear dynamical system. Furthermore, it has not processed in a unified method any poly-linear hysteresis characteristics (e.g., bi-linear and tri-linear, degrading tri-linear types). In contrast, the proposed method enables automatically determining the column basis of a matrix **A** from the response data by representing the restoring force as Eq. (3). It does not necessitate the selection and assumption of a basis function system. In addition, any poly-linear hysteresis characteristics can be addressed in a unified formula expression in Eqs. (2) and (3). These are the proposed method's most significant features and advantages, which differ from previous research. The column rank of a matrix **A** represents the degrees of freedom of the model and is closely related to the representational capability of the linear mapping in Eq. (4). The higher the column rank, the more complicated nonlinear characteristics that can be represented, but it also includes the problem of fitting to physically meaningless data (e.g., measurement noise). Furthermore, since Eq. (4) is an under-determined equation (unknowns are much relative to the number of independent equations), more than one candidate solution is possible. Then, the extraction of the critical components with a high contribution to the equation is processed, assuming the sparsity (many components of the solution vector are 0) in the solution of Eq. (7) and applying dimensional compression (sparse

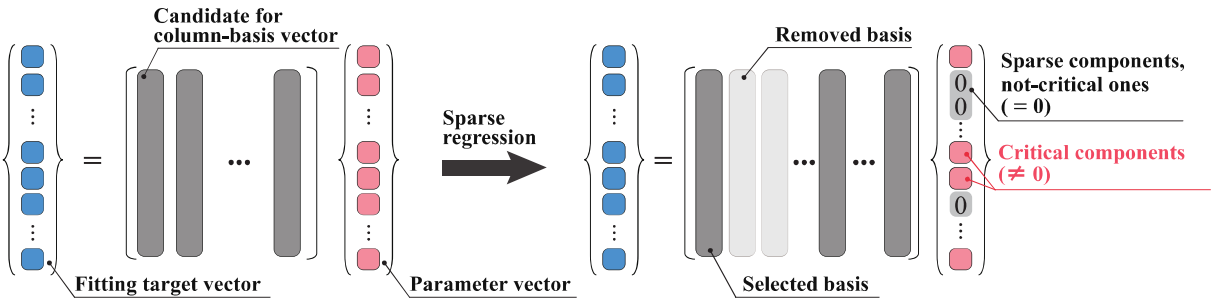

Figure 2 Conceptual diagram for sparse modeling

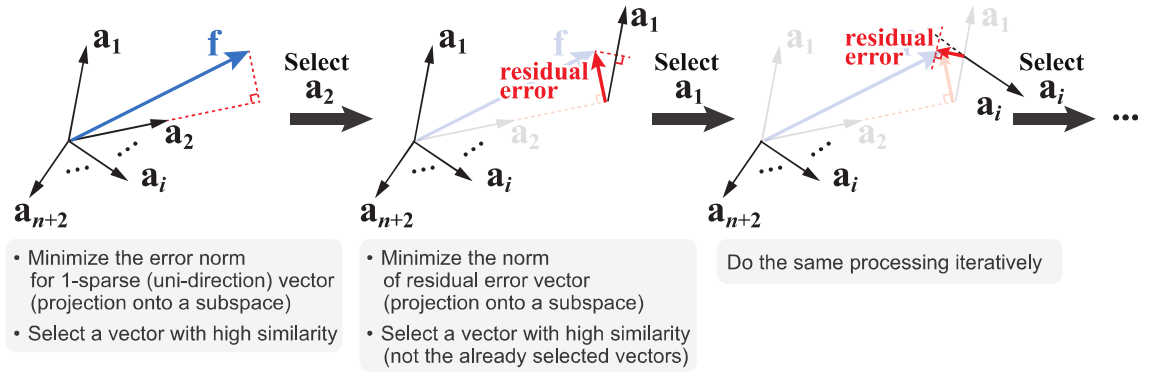

Figure 3 Conceptual diagram of iterative processing in the OMP method

modeling) as shown in Fig. 2. That means that the force equilibrium can be approximated using a simpler model (many of the stiffness changes Δk_i in Eq. (7) are zero). It also improves the robustness to noise by incorporating allowable tolerances (to be discussed later). This feature is expected by introducing sparse modeling into Eq. (7) and is independent of the previously described unified formulation of poly-linear type hysteresis characteristics.

It is possible to calculate the time-history variation of stiffness from Eq. (2) by providing the dynamic force f_i, relative displacement u_i, and relative velocity $\dot{u}_i$ and solving Eq. (4) under the assumption of solution sparsity. In this paper, the dynamic external force is the seismic story shear force, and the absolute acceleration responses of the building and the mass of each floor are known in the evaluation. The velocity will be integrated from the acceleration response through filtering using the Trifunac method[36] because the influence of the low-frequency components is relatively minor. The displacement estimation by filtering is difficult if there is a drift component (e.g., residual deformation), and the displacement is rarely obtained as the measurement data. Thus, there is a significant issue in making the displacement known, but this will be discussed in the future. Several methods for linear regression algorithms have been developed under the assumption of solution sparsity, and this paper adopts the Orthogonal Matching Pursuit (OMP) method. This method is a kind of greedy method, which iterates the problem of minimizing the squared error by a 1-sparse vector (with one nonzero component) as a partial optimization problem, as shown in Fig. 3. In the OMP method, the residual vector is projected onto each column vector, and the column vector with the smallest error norm is selected sequentially as the basis vector. It is a more efficient algorithm than the matching pursuit method with respect not to duplicating the selection of the basis. Although it does not always give a globally optimal solution, it is known as an effective method for l_0 optimization problems. The reasons for adopting this algorithm are as follows.

- The algorithm minimizes the l_0 norm (the number of nonzero components) with Eq. (4) as a restriction condition, as shown in Eq. (8).

$$\underset{\mathbf{p}\in\mathbb{R}^{n+2}}{\text{minimize}} \ \|\mathbf{p}\|_0 \quad \text{subject to } \mathbf{f} = \mathbf{A}\mathbf{p} \tag{8}$$

- No need to adjust hyperparameters, such as regularization coefficients as in l_1 and l_2 regularization.
- It is an easy-to-implement algorithm.
- If the matrix $\mathbf{A}$ is of full-row-rank, the upper limit number of iterative steps is automatically determined, and the convergence rate is first order. That is, the residue error decreases exponentially.

It is known that the OMP method can find the unique solution of Eq. (8) in a finite number of steps if there exists a sufficiently sparse solution **p** in equation **f − Ap=0** [32]. In addition, since the matrix **A** is of full-row-rank (= n+1 by Eq. (6)), the iterative computation is completed in Max. n+1 iteration steps and the convergence rate is first order; the residue error decreases exponentially. However, it should be noted that each step requires an inverse matrix computation, which can be a significant computation burden when the l_0 norm (the number of nonzero components) is enormous; that is, the less error norm ratio (defined later) is. In practical applications, the computational cost can be lower because a tolerance error is introduced to avoid overfitting, as shown below.

When applying the OMP in this paper, the following minimization problem will be solved by introducing an allowable tolerance $\varepsilon > 0$ to relax the equality constraint $\mathbf{f} = \mathbf{Ap}$, considering the influence of the noise. Among the candidate solutions, the sparsest solution **p** (the solution with the most zero components) with less than or equal to the allowable error will be selected as shown in Eq. (9).

$$\underset{\mathbf{p}\in\mathbb{R}^{n+2}}{\text{minimize}} \ \|\mathbf{p}\|_0 \quad \text{subject to} \ \|\mathbf{f}-\mathbf{Ap}\|_2 \le \varepsilon \tag{9}$$

As shown in Eq. (10), the tolerance ε is given by the l_2-norm ratio r to the dynamic force **f** (hereafter, the "error norm ratio"). It should be noted that the less the error norm ratio r, the better not only the compatibility with the equation but also the fitness to physically meaningless noise. The computation cost is also higher.

$$\varepsilon = \|\mathbf{f}-\mathbf{Ap}\|_2 = r\cdot\sqrt{\sum_{i=0}^{n} f_i^2} \tag{10}$$

The error norm ratio r balancing the fitness and the number of nonzero parameters will be determined based on the basic approach by the procedure indicated below.

Step 1 As shown in Fig. 4, plot the number of regression parameters and the RMS (Root Mean Square) of the residual error vs. threshold of error norm ratio r. When the error norm ratio r is larger, the number of parameters decreases, and the RMS error increases. If it is pattern A in Fig. 4, where a stable range exists, select the ratio in which the RMS of the residual error starts stabilizing for error norm ratio r. This is because the regression parameters as features are likely to be also stable for the range.

Step 2 In pattern B (see Fig. 4), where a stable range does not exist, select the ratio to maximize the length of the perpendicular line to a straight line that draws between the lower and upper bound of r.

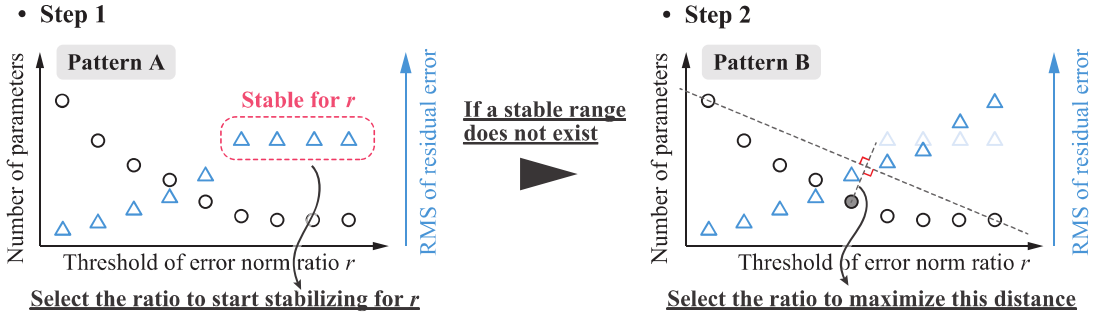

Figure 4 Procedure to determine error norm ratio r

VERIFICATION OF IDENTIFICATION ACCURACY BASED ON NUMERICAL ANALYSIS

Analysis conditions

The accuracy of the proposed method is investigated through numerical analysis. The response analysis model is a shear-type vibration model with a single degree of freedom (SDOF). Note that the application domain of the proposed method is not limited to SDOF systems. The hysteresis characteristics of the response analysis model are of two types: the normal bi-linear model (BL model) and the modified Takeda model[37] (MT model), which introduce the stiffness reduction during unloading and reloading, as shown in Fig. 5. The physical properties of the response analysis model are shown in Table 1. For both models, damping characteristics are assumed to be proportional to the initial stiffness, with a damping ratio of 2% for the BL model and 3% for the MT model. For both models, the mass m, initial stiffness

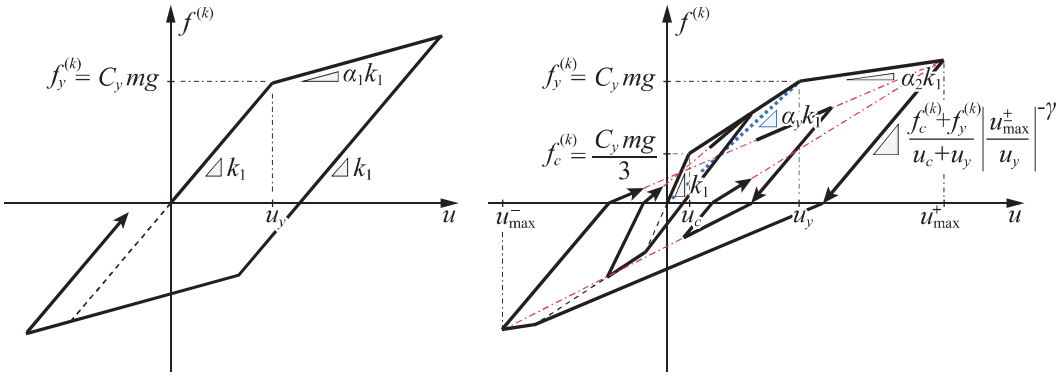

(a) Normal bi-linear model (BL model) (b) Modified Takeda model (MT model)

Figure 5 Hysteresis characteristics and each parameter

Table 1 Physical properties of the response analysis model

Hysteresis characteristics*1	Parameters*2							
	m [t]	k_1 [kN/m]	T_1 [s]	C_y [-]	h [-]	α_1 (α_y) | α_2 [-]	u_c | u_y [$\times 10^{-3}$ m]	γ [-]
BL model	100	43865	0.3	0.3	0.02	0.1 | -	- | 6.707	-
MT model					0.03	(0.3) | 0.001	0.2236 | 22.36	0.4

*1 See Fig. 5

*2 k_1, T_1, C_y : initial stiffness, initial natural period, yield shear force coefficient
α_1, α_y, α_2 : ratios of second stiffness, secant stiffness at yield, third stiffness to initial stiffness
u_c, u_y : deformation at cracking, yielding
γ : exponent representing stiffness degradation on unloading

k_1, initial natural-period T_1, and story shear coefficient at yielding C_y are 100 t, 43865 kN/m, 0.3 s, 0.3, respectively. The stiffness ratio of the BL model is $\alpha_1 = 0.1$, the stiffness ratios of the MT model are $\alpha_y = 0.3$ and $\alpha_2 = 0.001$, and the cracking and yielding displacements are determined accordingly. The unloading stiffness reduction index γ for the MT model is set to 0.4. The responses of the models are calculated with a time increment of 0.001 s using the Newmark-β method with γ=0.5 and β=0.25 (constant acceleration method), and El Centro 1940 NS is applied as the input earthquake ground motion. However, the resampling is performed at 0.01 s to lessen the computation costs for the identification. Response data generated under the analysis conditions above is regarded as measurement data and is used for identification. Furthermore, the band-limited white noise (0.1 Hz-25 Hz) is added to each response data to consider the influence of noise. The ratio of standard deviation to the responses before adding the noise is set to 0%, 1%, and 5% (hereinafter, "noise level"), and the signal-to-noise ratio is the same in each response.

Time series variation of story stiffness

The identification results for each model in a noise-free case are shown in Table 2 and Fig. 6. The error norm ratio r was set to a sufficiently small value (r = 0.001) because of the 0% noise level. In Table 2, the identified damping coefficient c is summarized. The bracket value indicates the identification value ratio to the setting value. The identification value corresponds well to the setting value of each model. In Fig.6, the top panel of the figure shows the identification results for the time series variation of story stiffness. For comparison, the response analysis results (forward analysis results) are shown as red lines, and the setting values for each model are shown as blue dashed lines. The bottom panel of the figure indicates the elastoplastic strain energy estimated from Eq. (11) using Eqs. (3) and (9). For comparison, the results of the forward analysis (Simu. in the figure) are also shown.

$$W_{es\&p} = \int_0^t f^{(k)} \dot{u} dt \tag{11}$$

The stiffness of the proposed method corresponds well to that of the forward analysis and the method has high accuracy, as shown in Fig. 6. The elastoplastic strain energy $W_{es\,\&\,p}$ exhibits the same trend. In particular, the results show good agreement during the time range (the blue dashed circles in the figure) when significant stiffness reduction and high hysteresis damping occur. These results support the theoretical validity of the proposed method.

The identification results for 1% and 5% noise levels are shown in Table 2, Figs. 7 and 8. In Table 2, the damping coefficient c, which was identified by applying the error norm ratio described later, corresponds well to the setting value of each model at the 1% noise level. However, the accuracy is much low at the 5% noise level and is influenced significantly by the noise. In Figs. 7 and 8, the top panel of each figure shows the number of model parameters and the RMS error vs. error norm ratio r. The threshold values for the error norm ratio were determined (indicated by ▼) based on "Step 2 (pattern B in Fig. 4)" in the procedure, as mentioned before. The middle and bottom panels of the figures represent the corresponding results. There is some time range in which the time variation of stiffness cannot be tracked, as shown in Figs. 7 and 8. However, there is good agreement with the results of the forward analysis in the time range (the blue dashed circle) when a significant stiffness reduction and high hysteresis damping occur. In other words, the stiffness change is generally well identified in the principal part where significant nonlinearization and hysteresis damping have occurred.

These results indicate that the proposed method can be helpful in damage detection by investigating the time series variation of stiffness. The applicability of the proposed method will be discussed in the following chapter through the correspondence with actual damage conditions using data from a full-scale shaking table test.

Table 2 Accuracy of identified damping coefficient c (kNs/m)

BL model *			MT model *		
Without noise	With noise		Without noise	With noise	
	Noise level 1%	Noise level 5%		Noise level 1%	Noise level 5%
84.0 (1.00)	88.0 (1.05)	115.3 (1.38)	126.1 (1.00)	132.1 (1.05)	161.8 (1.29)

* The value in bracket is the ratio of identificaton value to setting value

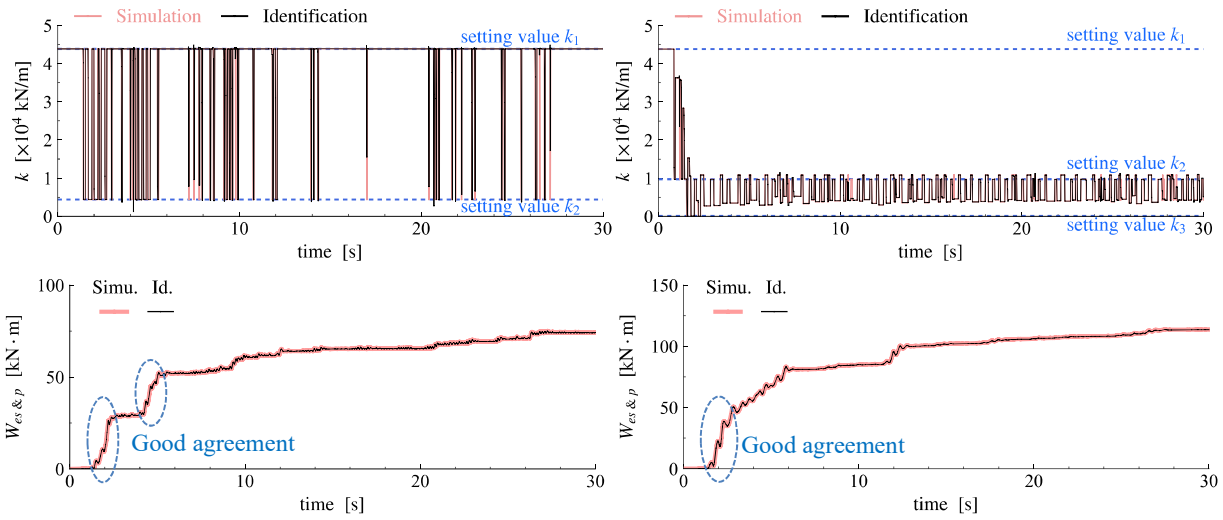

(a) BL model (b) MT model

Figure 6 Identification result without noise (r = 0.001). *Top panel*: Time series of identified story stiffness. *Bottom panel*: Elastic and plastic strain energy.

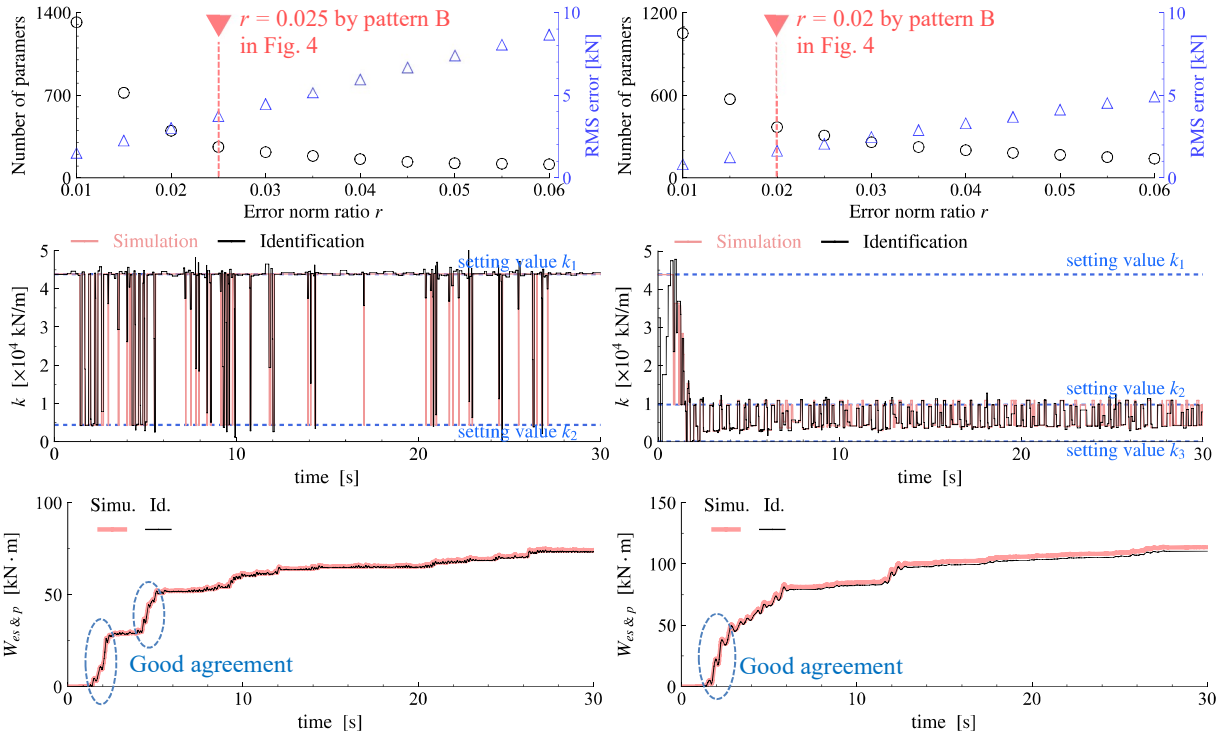

Figure 7 Identification result for 1 % noise level. *Top panel*: Adopted error norm ratio *r*. *Middle panel*: Time series of identified story stiffness. *Bottom panel*: Elastic and plastic strain energy.

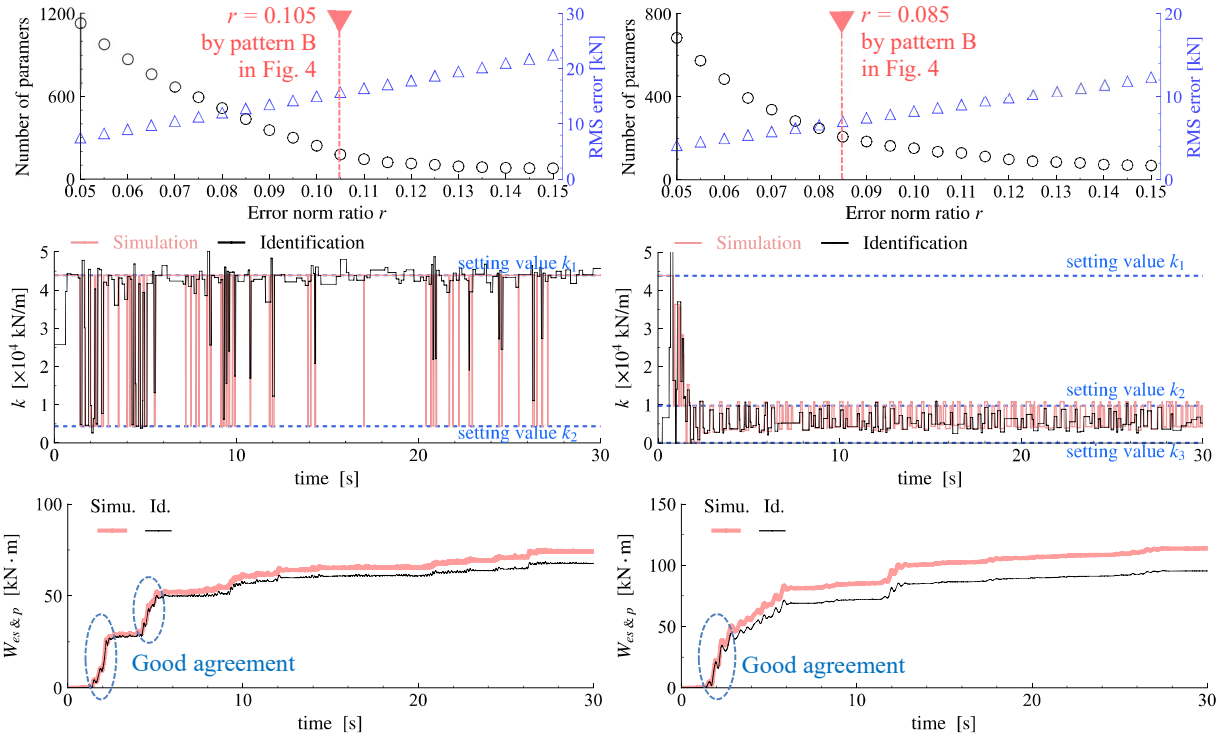

Figure 8 Identification result for 5 % noise level. *Top panel*: Adopted error norm ratio *r*. *Middle panel*: Time series of identified story stiffness. *Bottom panel*: Elastic and plastic strain energy.

VERIFICATION OF IDENTIFICATION METHOD BASED ON FULL-SCALE SHAKING TABLE TEST

Test specimens and experimental summary[38-42)]

The validity of the proposed method will be verified using measurement data[38)] from a seismic shaking table test conducted on a 3-D Full-Scale Earthquake Testing Facility (nicknamed "E-Defense") owned by the National Research Institute for Earth Science and Disaster Resilience (NIED). The tests applied for verification are a collapse test of a full-scale four-story steel structure building (hereinafter, S4) conducted in 2007[39,40)] and a test of a full-scale three-story steel structure building (hereinafter, S3) conducted in 2013[41)]. A panoramic view of each test specimen is shown in Fig. 9, and the excitation cases discussed in this paper are listed in Table 3.

The test specimen S4 consists of 6 m × one span in the X-direction (the shorter direction) and 5 m × two spans in the Y-direction (the longer direction). The story heights are 3.875 m for the first floor and 3.50 m for the second to fourth floors. The building's height is about 14 m. The building is a frame structure in both the X and Y directions. The input earthquake ground motions used in the shaking tests are the JR Takatori station record (hereinafter, Takatori) of the 1995 Hyogo-ken-Nanbu earthquake, with EW, NS, and UD components in the X, Y, and Z directions, respectively. The acceleration scaling factor adjusted the excitation level relative to the original wave. Tests were conducted by varying the scaling factor in the following order: 5%, 10%, 12.5% (first), 20%, 12.5% (second), 40%, 60%, 100%, etc. The excitation levels discussed in this paper are 20%, 40%, and 60%, and the studied direction is in the X-direction. The reason for excluding 100% is that displacement data were unavailable for some periods, and the data required for identification was insufficient. In these excitation levels, input compensation control[42)] was applied to improve the reproducibility of the input ground motions, and it was noted that the influence (e.g., input energy loss) associated with shaking-table rocking is minor[39)].

The test specimen S3 consists of 5 m × two spans in the X-direction (the shorter direction) and 6 m × two spans in the Y-direction (the longer direction). The story heights are 3.8 m for the first floor and 3.475 m for the other floors. The building's height is about 11 m. The test specimen was designed to focus on a single frame of a three-story steel structural building, and the central vertical plane in Y-direction was a principal test target. Only this vertical plane is a frame structure, while the two outers are vertically supported by columns with pin joints at both ends and do not bear horizontal forces. The excitation was one-directional horizontal excitation in the Y-direction only. The X-direction is orthogonal to the direction of excitation and is a braced structure to prevent torsional deformation. The input earthquake ground motions used in the tests are the assumed Nankai Trough earthquake ground motion and the Takatori (NS component). Since significant damage (e.g., beam end fracture) was observed for the first time at the Takatori input[38,41)], this paper focuses only on the Takatori input and covers all excitation levels (40%, 60%, 80%, and 100%). The input ground motion was highly reproducible although no input compensation control was used for these excitations [38)].

(a) Four-story steel structure building (S4) (b) Three-story structure building (S3)

Figure 9 Panoramic view of each test specimen

Table 3 Excitation cases used for identification in each test specimen

S4		S3	
Excitation case	PGA* in X-dir. [gal]	Excitation case	PGA* in Y-dir. [gal]
Takatori 20%	143	Takatori 40%	246
40%	350	60%	378
60%	551	80%	542
		100%	714

* Max. value of the time series waveform averaged over accelerations at 1FL

Responses used for identification and their preprocessing

As described in the previous chapter, the following data were required to identify each story stiffness by the proposed method: (1) the shear force in each story, (2) the inter-story drift, and (3) the inter-story velocity. First, the measured absolute acceleration response and the masses at each floor shown in Table 4 were used to determine (1). Next, the measured story drift data were used as (2). Finally, the acceleration responses were integrated using the Trifunac method[36] to calculate (3). It should be noted that the filter parameters of the Trifunac method were adjusted based on the frequency transfer function of the observed response to the input ground motion.

Table 4 Floor mass of each specimen [38]

S4		S3	
j th FL	mass [t]	*j* th FL	mass [t]
2FL	48.4	2FL	44.9
3FL	48.2	3FL	43.9
4FL	48.6	RFL	40.6
RFL	64.4		

A high-cut filter was applied to the data obtained in the above process to lessen the influence of noise on the identification results. This paper removes the frequency components after the third-order dominant frequency of each specimen (consistently after 10 Hz). Furthermore, when the normalized cumulative power $P_C(t_0, t_n)$ defined in Eq. (12) is 1%–95%, the time range (t_0-t_n) was set as the section to be identified (time range in equation (4)). This is the purpose of removing microtremors before shaking and using data with a relatively high signal-to-noise ratio. The absolute acceleration response of the top floor was used for the signal $g(t)$.

$$P_C(t_0, t_n) = \frac{\int_{t_0}^{t_n} g(t)^2 dt}{\int_0^{\text{Measurement end time}} g(t)^2 dt} \tag{12}$$

The sampling frequency was reduced from 1000 Hz (the measurement sampling frequency for each test) to 100 Hz, and the identification was performed after resampling to lessen computation costs.

Identification result

Figs. 10 a–c show the number of model parameters and the RMS error vs. error norm ratio r for the first to third stories under Takatori-20% excitation, respectively, as examples. The threshold values for the error norm ratio were determined (indicated by ▼) based on "Step 1 (pattern A in Fig. 4)" in the procedure, as mentioned before. The threshold values are the same through all excitation levels to make a comparison between excitation levels clear.

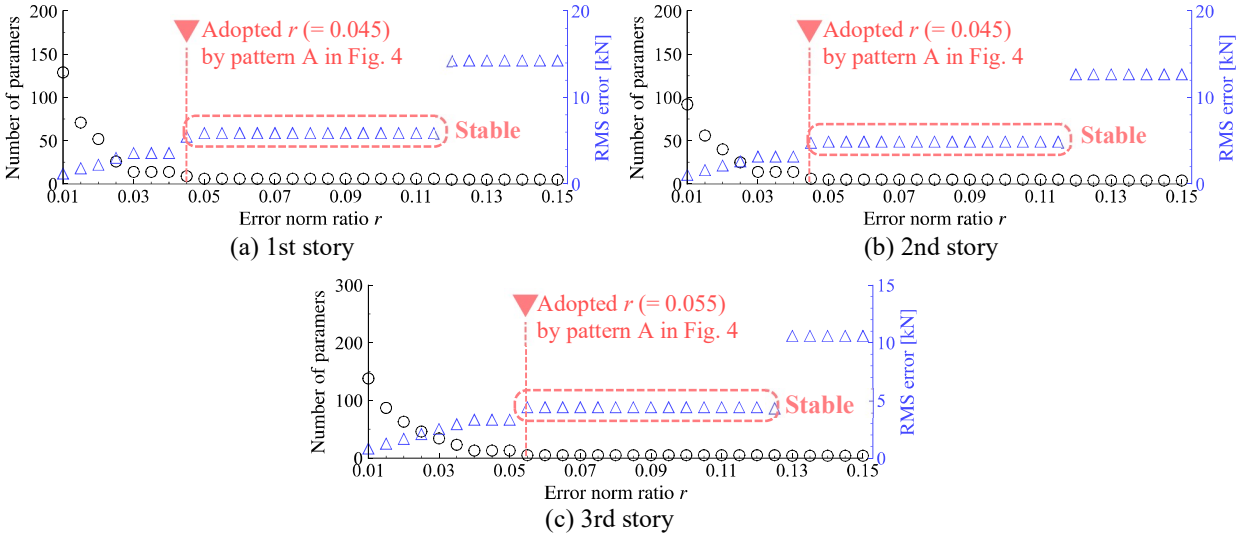

Figure 10 Adopted error norm ratio r (S4, Takatori-20)

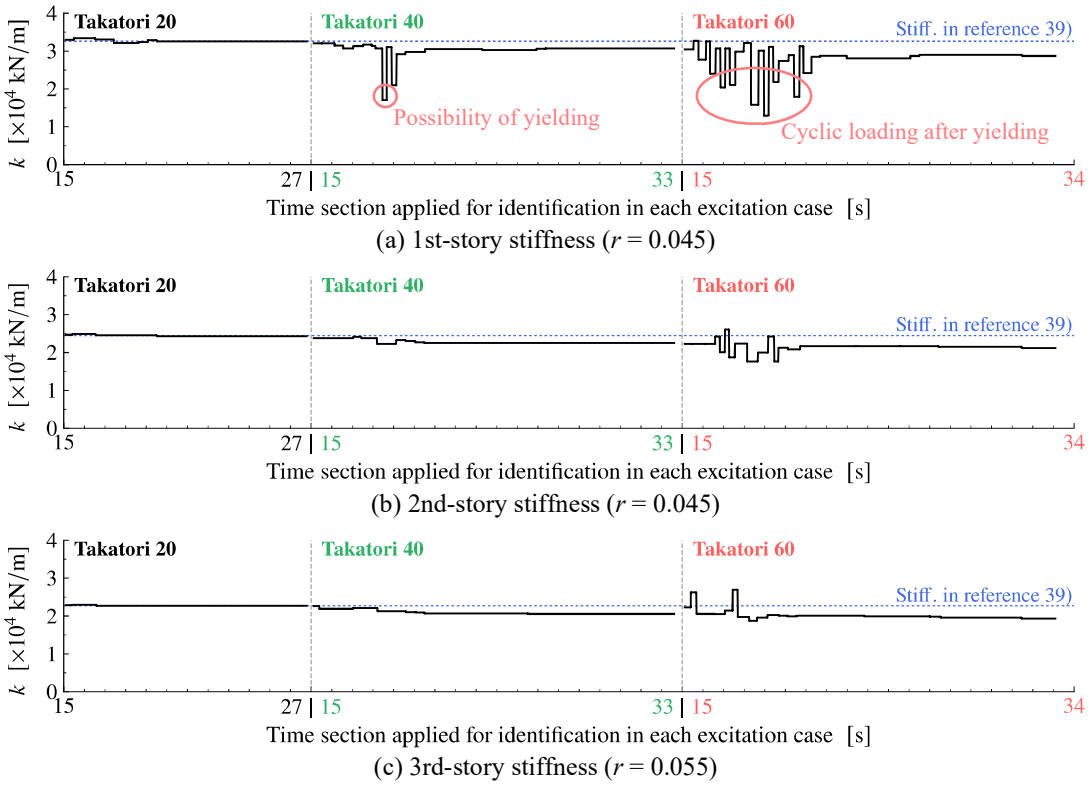

Figure 11 Time series of story stiffness identified for each excitation case in specimen S4

Figs.11a–c show the results of identifying the story stiffness in specimen S4 for the first to third stories, respectively. In each figure, the results for each excitation level are summarized. The blue dashed line in Fig. 11 indicates the story stiffness of the entire specimen in reference[39] for Takatori-20% excitation as a comparison value. According to the same reference, it is noted that the structure exhibited linear behavior under 20% excitation. The identification results under 20% excitation correspond well to the previous research's identification results[39] (blue dashed line), as shown in Fig. 11. Furthermore, the story stiffness has a nearly constant tendency, indicating that it is in the linear response range, as mentioned in reference[39]. The identification results for the Takatori-40% excitation show a tendency for the first story stiffness to recover gradually after stiffness reduction (red circle in the figure). The structural members

likely experienced the yielding. It is mentioned in reference [40] that the top of some columns and the bottom of all columns in the first story experienced full plasticity under the Takatori 40% excitation. This would correspond to the tendency of the identification results in the first story. However, it has not fully recovered toward the stiffness identified at the early Takatori-40% excitation. Since the stiffness of pure steel components that yielded will recover after loading, such no full stiffness recovery is most probably due to the cracking of RC floor slabs, which contributes to the story stiffness as well[43]. Although there is no significant decrease in stiffness in the other stories, the stiffness tends to decrease slightly over time. In the Takatori 60% excitation identification results, the stiffness variation is prominent in the first story, which likely indicates the influence of cyclic behavior after yielding. According to reference[40], the top and bottom of all columns in the first story and all beam-to-column joints on the second floor experienced full plasticity under the Takatori 60% excitation. The cracking of RC floor slabs on the second and third floors is also reported. That is likely why the identification results show a significant stiffness change, as shown in Fig.11a. Furthermore, in the same reference, it is mentioned that one beam-to-column joint on the third-floor experienced full plasticity. This influence is most probably reflected in the stiffness changes of the second and third stories (Figs. 11b and c). In Fig. 11c, although the stiffness of the third story is greater than its initial stiffness, it is likely not to indicate any physical meaning. Since the proposed method does not directly impose a constraint condition between the regression parameters (**p** in Eq. (7)), this influence appeared likely as an identification error. However, the influence of an identification error such as this case would be practically minor on damage detection because notable damage is detected most probably by the relationship between the initial and final identification values or the intense variation (decrease/increase) in stiffness with loading/unloading during an earthquake. Figs. 12 and 13 show examples of shear force vs. story drift estimated using the identified parameters. The figures show good correspondence with the experimental results, implying that the identification was conducted appropriately. The experimental hysteresis was derived by the measured accelerations, the measured inter-story drift and the masses at

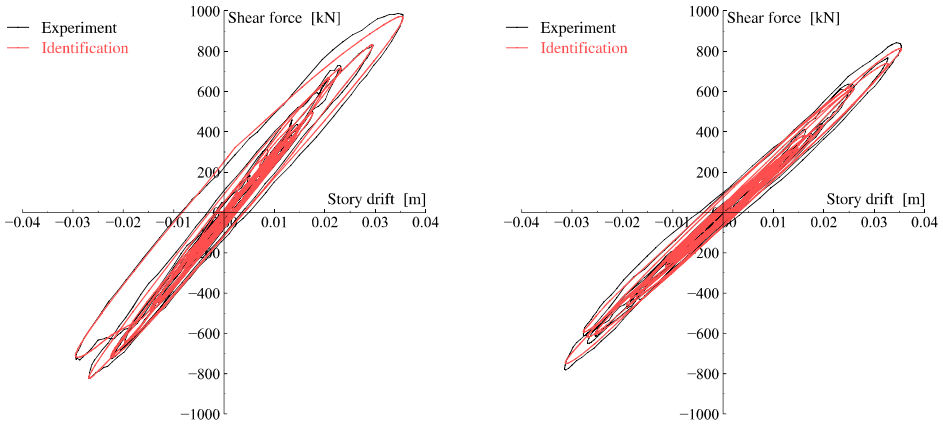

(a) 1st story (b) 2nd story

Figure 12 Story shear force vs. story drift estimated based on the identified time-varying stiffness (S4, Takatori-40)

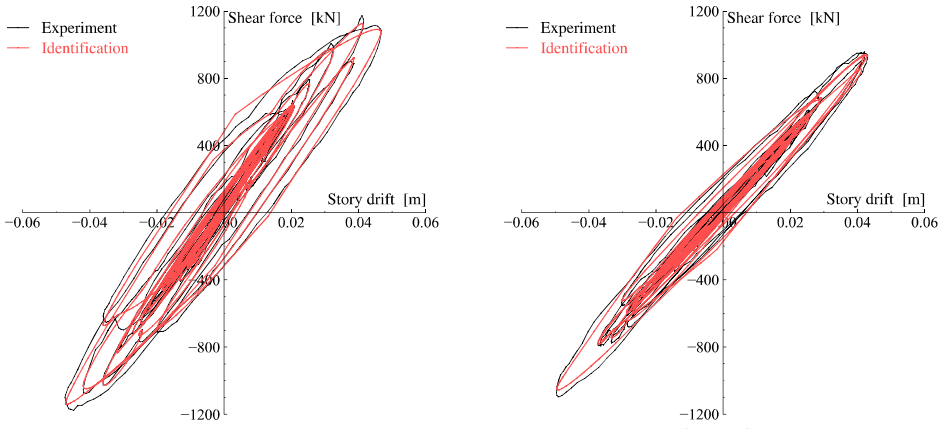

(a) 1st story (b) 2nd story

Figure 13 Story shear force vs. story drift estimated based on the identified time-varying stiffness (S4, Takatori-60)

Table 5 Accuracy of identified damping coefficient c (kNs/m) in S4 specimen

Excitation case		Damping coefficient by this paper / by Ref.[29, 30] (Ratio to damping coefficient by Ref.[29, 30])			
		Story 1	Story 2	Story 3	Story 4
Takatori	20	354.1 / 353.6 (1.00)	268.2 / 273.3 (0.98)	237.4 / 240.2 (0.99)	300.5 / 281.2 (1.07)
	40	361.0 / 323.9 (1.11)	296.3 / 270 (1.10)	243.7 / 240.5 (1.01)	259.2 / 233.0 (1.11)
	60	360.7 / 760.3 (0.47)	287.4 / 404.2 (0.71)	226.1 / 268.8 (0.84)	231.2 / 244.9 (0.94)

each floor in Table 4, as mentioned in the section "Responses used for identification and their preprocessing". The same process will be applied to the S3 specimen in the later. The identified damping coefficients are summarized in Table 5. Table 5 shows the values identified in previous research[29,30] and their ratios. Each story's damping coefficients generally correspond to the identification results of previous research at Takatori 20 and 40, but it has a low agreement at Takatori 60. The reference [29] reports that the validity of the separation of viscous and hysteresis damping may not apparent, and it can be a future issue in this research as well.

Figs. 14a, b show the number of model parameters and the RMS error vs. error norm ratio r for the first to third stories in the S3 specimen under Takatori-40% excitation, respectively, as examples. The error norm ratios were determined (indicated by ▼) in the same way as the S4 specimen. Figs. 15a, b show the results of identifying the story stiffness of the first and second stories in specimen S3. Also, the figures show the equivalent stiffness (gray dashed line) calculated by applying the least-squares method to the force-deformation curve for the Takatori-40% excitation. From Fig. 15, the least-squares method and the identification results correspond well and exhibit a generally constant trend, implying that the response is generally within the linear range at 40% excitation. This corresponds to experimental reports in reference [41]. The identification results for the Takatori-60% excitation show a tendency for the first- and second-story stiffnesses to recover mostly after decreasing (red circle in the figure), implying that yielding has occurred. However, it has not fully recovered toward the stiffness identified at the early Takatori-60% excitation. Such no full stiffness recovery is most probably due to the cracking of RC floor slabs, which contributes to the story stiffness as well[43]. In reference[41], it is mentioned that the bottom flange of the beam ends at the second and third floors plasticized under 60% excitation, and the cracking of RC floor slabs is also reported. These are likely reflected in the identification results. Takatori-80% excitation results show a more noticeable stiffness variation than 60% excitation, implying that plasticization advances because of cyclic behavior. In Takatori-100% excitation, a significant decrease in stiffness occurs around 14 s after the shaking, along with a noticeable stiffness variation. The story stiffnesses have decreased by approximately 50% when compared with the early period of 100% excitation. According to reference[41], the bottom flange of the beam end on the second floor ruptured, and local buckling occurred 13 to 14 s after the shaking. The stiffnesses of the first and second stories (just upper and lower than the floor with the damaged beam) significantly decrease in identification results, corresponding well to the reported damage conditions[41]. Figs. 16 and 17 show examples of shear force vs. story drift estimated using the identified parameters. The figures indicate good agreement with the experimental results, implying that the identification was conducted appropriately. The proposed method is generally reliable for damage detection because the tendency of damage in the experiment generally corresponds to the identification results. Note that for the S3 specimen, the identified damping coefficients are not listed because no previous research's results to compare the identification accuracy was not found.

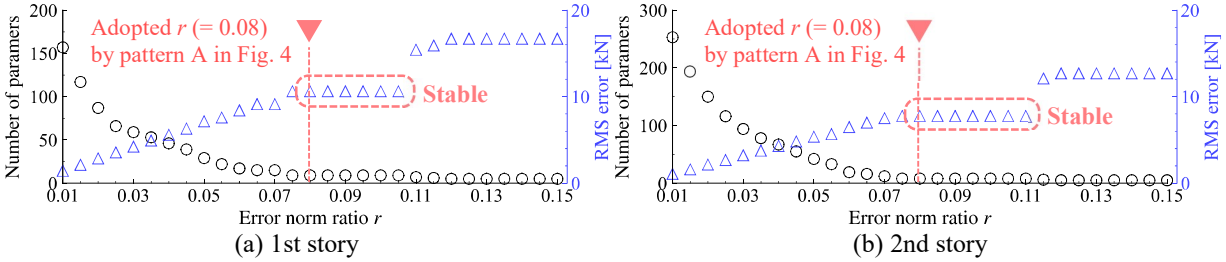

(a) 1st story (b) 2nd story

Figure 14 Adopted error norm ratio r (S3, Takatori-40)

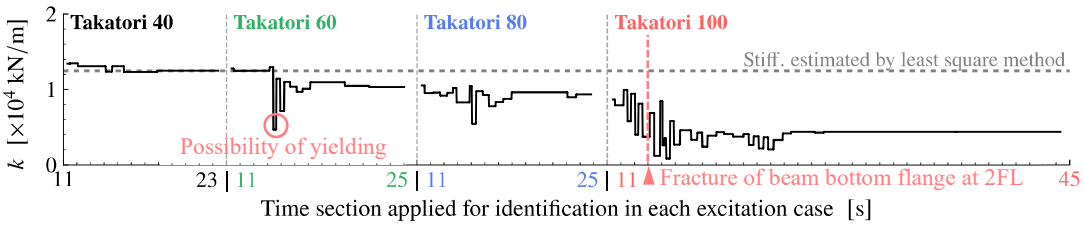

(a) 1st-story stiffness (r = 0.08)

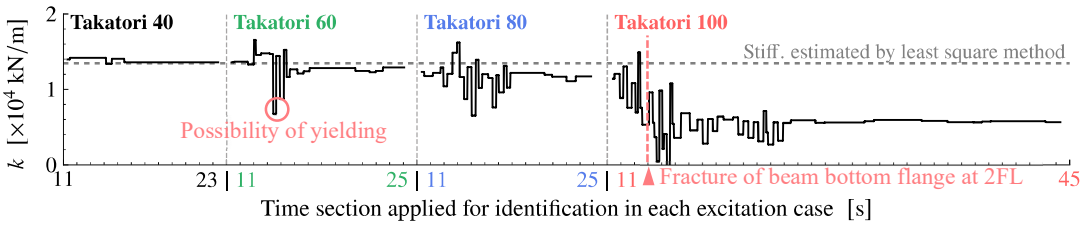

(b) 2nd-story stiffness (r = 0.08)

Figure 15 Time series of story stiffness identified for each excitation case in specimen S3

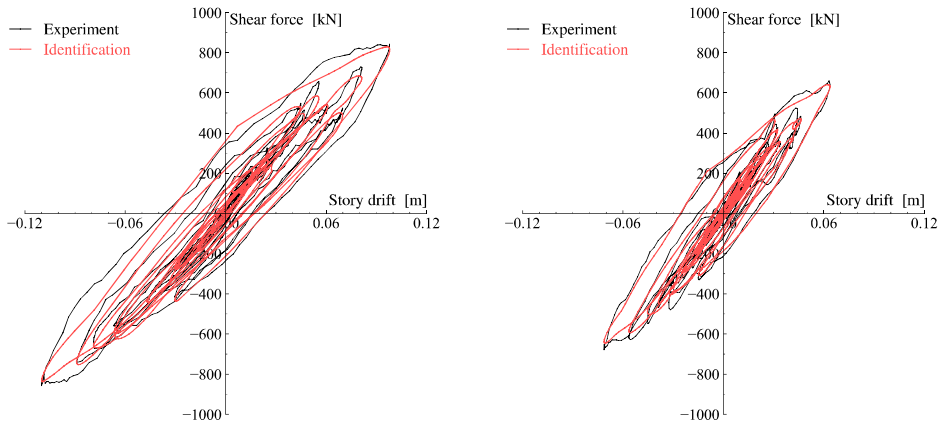

(a) 1st story (b) 2nd story

Figure 16 Story shear force vs. story drift estimated based on the identified time-varying stiffness (S3, Takatori-80)

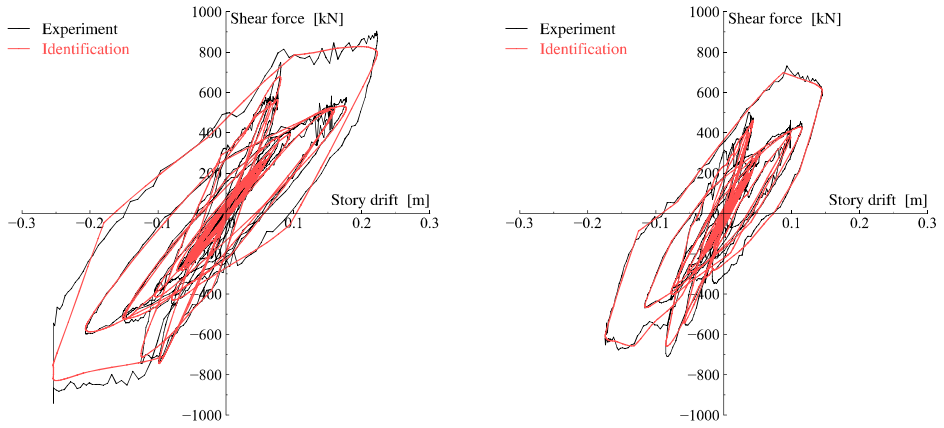

(a) 1st story (b) 2nd story

Figure 17 Story shear force vs. story drift estimated based on the identified time-varying stiffness (S3, Takatori-100)

CONCLUSIONS

A stiffness identification method in the time domain applicable to structures with arbitrary poly-linear hysteresis characteristics is developed in this paper. The validity of the proposed method was demonstrated through numerical analysis and full-scale shaking table tests. The conclusions are summarized as follows.

- The force equilibrium equation was expressed explicitly regarding the amount of stiffness change, and a new linear regression problem applicable to poly-linear hysteresis characteristics was developed. Furthermore, a stiffness identification method in the time domain based on a unified expression was developed by introducing sparse modeling and minimizing the l_0 norm. This allows for detecting critical stiffness changes that significantly contribute to the force equilibrium. In addition, the proposed method eliminates the need to select the basis function system (the function system that composes the fitting target), which is found in previous research, because the coefficient matrix of the regression problem can be determined automatically from the response data.
- The validity of the proposed method was simulated numerically for models that exhibit bi-linear and modified Takeda hysteresis characteristics. The theoretical validity of the proposed method was confirmed by the fact that the identified story stiffnesses agree well with the setting values in noise-free cases. Furthermore, although the identification accuracy slightly deteriorates in the case of noise, the yielding and stiffness-variation are identified well in the time range when significant stiffness reduction and large hysteresis damping occur.
- The proposed method was demonstrated using full-scale shaking table test data on two steel structure specimens, S3 and S4. The decrease in story stiffness with increasing excitation level was apparent, and it was also confirmed that the damage condition in the experiment generally corresponded to the identified results. Furthermore, the post-yielding story stiffness tended to gradually recover toward the value identified at the early excitation period after stiffness reduction. This tendency was the same for both specimens. On the other hand, as indicated in the excitation experiment for S3, the stiffness recovery tendency did not appear when the beam-end fracture occurred. In addition, the stiffnesses significantly decreased in stories just above and below the floor with the beam-end fracture. These results indicate that the proposed method is qualitatively valid for damage detection.

In evaluating modal property change during nonlinear response, the method by time series model (i.e., ARX model, multivariable subspace model) is not easy generally to set appropriate parameters (i.e., system orders, number of time segments, forgetting factor, number of block rows in block Hankel matrix ...) that balance between the time resolution and identification accuracy. The setting significantly impacts the results. Also, since the hysteresis curve involves the damping force, the stiffness changes hiding in hysteresis curves are not always easy to detect, even if the hysteresis curve is given. The proposed method detects characteristic stiffness changes by separating the story shear force into the damping force and restoring force through sparse modeling. These can be the additional benefit of using the proposed method for damage detection while the assumption of damping force remains an issue.

On the other hand, the proposed method does not incorporate processing to separate the rotational and shear-type responses. Therefore, it is difficult to apply to structures that exhibit rotational response rather than just shear-type response, such as a tall building utilizing a wall system. In addition, since the proposed method detects characteristic stiffness change points, the accuracy decreases likely for a model that shows a slow change in stiffness between elastic and inelastic behavior, such as Ramberg Osgood hysteretic material. These potential issues will be pursued in future work. Furthermore, to relax the assumption that c is constant, it is possible that the proposed method is applied after dividing the data into multiple time segments, but how to determine the time segments will be a problem. This problem will also be investigated in future work. Finally, making the displacement known is a significant issue in this paper. A displacement estimation cannot be avoided currently when the proposed method is applied to real structures. In recent research, since the displacement estimation method that considers drift components has been developed (for example, reference [44]), the accuracy and practice of the proposed method will be demonstrated in combination with such a method.

ACKNOWLEDGMENTS

This work utilized the experimental data provided by the Archives of Shakingtable Experimentation Database and Information (ASEBI) of E-Defense and was supported by JSPS KAKENHI Grant No. 22K14363. I gratefully acknowledge the JSPS, the Hyogo Earthquake Engineering Center, National Research Institute for Earth Science and Disaster Resilience (NIED) that manages E-Defense.

REFERENCES

1) Doebling SW, Farrar CR, Prime MB and Shevitz DW. Damage identification and health monitoring of structural and mechanical systems from changes in their vibration characteristics: A literature review. Report LA-12767-MS. Los Alamos National Laboratory. 1996. https://doi.org/10.2172/249299

2) Bendat JS and Piersol AG. Random data analysis and measurement procedures 4th edition. John Wiley and Sons Inc. New York. 2010.2

3) Safak E. Adaptive modeling, identification, and control of dynamic structural systems I: theory. *Journal of Engineering Mechanics*, ASCE. 1989;115(11):2386. https://doi.org/10.1061/(ASCE)0733-9399(1989)115:11(2406)

4) Ghanem R and Shinozuka M. Structural-system identification I: Theory. *Journal of Engineering Mechanics*, ASCE, 1995;121(2):255–264. https://doi.org/10.1061/(ASCE)0733-9399(1995)121:2(255)

5) Shinozuka M and Ghanem R. Structural-system identification II: Experimental verification. *Journal of Engineering Mechanics*, ASCE, 1995;121(2):265–273. https://doi.org/10.1061/(ASCE)0733-9399(1995)121:2(265)

6) Liu PL. Identification and damage detection of trusses using modal data. *Proc of the Second World Conference on Structural Control.* 1995;121(4):599–608. https://doi.org/10.1061/(ASCE)0733-9445(1995)121:4(599)

7) Hjelmstad KD. On the uniqueness of modal parameter estimation. *J Sound Vib.* 1996;192(2):581–598. https://doi.org/10.1006/jsvi.1996.0205

8) Hart GC and Yao JTP. System identification in structural dynamics. *J. Eng. Mech. Div.* 1997;103(6):1089–1104. https://doi.org/10.1061/JMCEA3.0002299

9) Nagarajaiah S, and Basu B. Output only modal identification and structural damage detection using time frequency & wavelet techniques. *Earthquake Eng. Eng. Vib*. 2009;8(4):583–605. https://doi.org/10.1007/s11803-009-9120-6

10) Takewaki I and Nakamura M. Stiffness-damping simultaneous identification under limited observation. *J Eng Mech*. 2005;131(10):1027–1035. https://doi.org/10.1061/(ASCE)0733-9399(2005)131:10(1027)

11) Zhang D and Johnson E. Substructure identification for shear structures I: Substructure identification method. *Struct Control Health Monit*. 2013;20(5):804–820. https://doi.org/10.1002/stc.1497

12) Wojtkiewicz S and Johnson E. Efficient sensitivity analysis of structures with local modifications I: Time domain responses. *J Eng Mech*. 2014;140(9). https://doi.org/10.1061/(ASCE)EM.1943-7889.0000768

13) Johnson E and Wojtkiewicz S. Efficient sensitivity analysis of structures with local modifications II: Transfer functions and spectral densities. *J Eng Mech*. 2014;140(9). https://doi.org/10.1061/(ASCE)EM.1943-7889.0000769

14) Suzuki Y, Adachi N, Ikeura T, et al. Prediction of artificial seismic damage of an actual building at a steel beam based on forced vibration test and microtremor. *AIJ Journal of Technology and Design*. 2010;16(33):473-478. https://doi.org/10.3130/aijt.16.473 (in Japanese)

15) Xie L, Mita A, Luo L, and Feng MQ. Innovative substructure approach to estimating structural parameters of shear structures. *Struct Control Health Monit*. 2018;25(4):e2139. https://doi.org/10.1002/stc.2139

16) Loh CH and Tsaur YH. Time domain estimation of structural parameters. *Eng Struct*. 1988;10(2):95-105. https://doi.org/10.1016/0141-0296(88)90035-1

17) Zhang C, Huang JZ, Song GQ and Chen L. Structural damage identification by extended Kalman filter with *l*1-norm regularization scheme. *Struct Control Health Monit*. 2017;24(11):e1999. https://doi.org/10.1002/stc. 1999

18) Yang JN, Lin S, Huang H and Zhou L. An adaptive extended Kalman filter for structural damage identification. *Struct. Control Health Monit.* 2006;13(4):849–867. https://doi.org/10.1002/stc.84

19) Xie L, Zhou Z, Zhao L, et al. Parameter identification for structural health monitoring with extended Kalman filter considering integration and noise effect. *Applied Sciences.* 2018;8(12):2480. https://doi.org/10.3390/app8122480

20) Enokida R and Kajiwara K. Simple piecewise linearization in time series for time domain inversion to estimate physical parameters of nonlinear structures. *Struct Control Health Monit.* 2020;27(10):e2606. https://doi.org/10.1002/stc.2606

21) Wen YK. Method for random vibration of hysteretic systems. *J Eng Mech*, ASCE. 1976;102(2): EM2-249. https://doi.org/10.1061/JMCEA3.0002106

22) Baber TT and Wen YK. Random vibration of hysteretic degrading systems. *J Eng Mech*, ASCE. 1981;107(6): 1066-1069. https://doi.org/10.1061/JMCEA3.0002768

23) Hoshiya M and Saito E. Identification problem of some seismic systems by extended Kalman filter. *Proc. Jpn. Soc. Civ. Eng*. 1983;339:59-67. https://doi.org/10.2208/jscej1969.1983.339_59 (in Japanese)

24) Hoshiya M and Maruyama O. Identification of restoring force characteristics of nonlinear systems during earthquakes. *Proc Jpn Soc Civ Eng.* 1987;386:397-405. https://doi.org/10.2208/jscej.1987.386_397 (in Japanese)

25) Agbabian MS, Masri SF, Miller RK, and Caughey TK. System identification approach to detection of structural changes. *J Eng Mech.* 1991;117(2):370-390. https://doi.org/10.1061/(ASCE)0733-9399(1991)117:2(370)

26) Loh CH and Chung ST. A three-stage identification approach for hysteretic systems. *Earthquake Eng Struct Dyn*. 1993;22(2):129-150. https://doi.org/10.1002/eqe.4290220204

27) Smyth AW, Masri SF, Chassiakos AG, and Caughey TK. On-line parametric identification of MDOF nonlinear hysteretic systems. *J Eng Mech.* 1999;125(2):133-142. https://doi.org/10.1061/(ASCE)0733-9399(1999)125:2(133)

28) Xu C, Chase JG, and Rodgers GW. Physical parameter identification of nonlinear base-isolated buildings using seismic response data. *Comput Struct*. 2014;145:47-57. https://doi.org/10.1016/j.compstruc.2014.08.006

29) Ikeda Y. Verification of identification methods for linear systems utilizing shaking table tests of full-scale 4-story steel building. *AIJ Journal of Technology and Design* 2010;16(34):889–894 (in Japanese).

30) Ikeda Y. Verification of system identification utilizing shaking table tests of a full-scale 4-story steel building, *Earthquake Eng Struct Dyn.* 2016;45(4):543-562. https://doi.org/10.1002/eqe.2670

31) Uesaka T, Nabeshima K, Nakamura N and Suzuki T. Physical parameters identification for full-scale ten-story reinforced concrete building with degrading tri-linear model by modal iterative error correction method. *Earthquake Eng Struct Dyn.* 2021;51(1):153-168. https://doi.org/10.1002/eqe.3560

32) Elad M. Sparse and Redundant Representations: From Theory to Applications in Signal and Image Processing. 1st ed. Springer, New York, 2010. https://doi.org/10.1007/978-1-4419-7011-4

33) Rudy SH, Brunton SL, Proctor JL and Kutz JN. Data-driven discovery of partial differential equations. Sci Adv 2017;3(4):e1602614. https://doi.org/10.1126/sciadv.1602614

34) Mangan NM, Kutz JN, Brunton SL and Proctor JL. Model selection for dynamical systems via sparse regression and information criteria. Proceedings of the Royal Society A: Mathematical, Physical and Engineering Sciences 2017;473(2204):20170009. 20170009. https://doi.org/10.1098/rspa.2017.0009

35) Guo J, Wang L, Fukuda I, Ikago K. Data-driven modeling of general damping systems by k-means clustering and two-stage regression. *Mech Syst Signal Process*. 2022;167:108572. https://doi.org/10.1016/j.ymssp.2021.108572

36) Trifunac MD. Low frequency digitization errors and a new method for zero baseline correction of strong-motion accelerograms, Report No.EERL 70-07, Earthquake Engineering Research Laboratory, California Institute of Technology, 1970.9

37) Takeda T, Sozen MA, Nielsen NN. Reinforced concrete response to simulated earthquakes. *J Struct Div.* 1970; 96(12):2557- 2573. https://doi.org/10.1061/JSDEAG.0002765

38) Hyogo Earthquake Engineering Center, National Research Institute for Earth Science and Disaster Resilience (NIED), ASEBI: Archives of E-Defense Shakingtable Experimentation Database and Information. https://doi.org/10.17598/nied.0020 [accessed September 1, 2022]

39) Suita K, Matsuoka Y, Yamada S, et al. Experimental procedure and elastic response characteristics of shaking table test: Complete collapse test of full-scale 4-story steel building part 1. *Journal of Structural and Construction Engineering* (Transactions of AIJ). 2009;74(635):157-166. https://doi.org/10.3130/aijs.74.157 (in Japanese)

40) Yamada S, Suita K, Matsuoka Y and Shimada Y. Elasto-plastic responses and process leading to a collapse mechanism: Dynamic collapse test of full-scale 4-story steel building part 2. *Journal of Structural and Construction Engineering* (Transactions of AIJ), 2009;74(644):1851-1859. https://doi.org/10.3130/aijs.74.1851 (in Japanese)

41) Mizushima Y, Mukai Y, Namba H, et al. Super-detailed fem simulations for full scale steel structure caused fatal rupture at its joint parts between members: Shaking table test of full scale steel frame structure to estimate influence of cumulative damage by multiple strong motion part 1. *Journal of Structural and Construction Engineering* (Transactions of AIJ). 2016;81(719):61-70. https://doi.org/10.3130/aijs.81.61 (in Japanese)

42) Yamada S, Maezawa M, Mori T, et al. Evaluation of performance check on E-Defense based on the energy input, *Journal of Structural and Construction Engineering* (Transactions of AIJ). 2007;72(512):207-214. https://doi.org/10.3130/aijs.72.207_1 (in Japanese)

43) Ji X, Fenves GL, Kajiwara K and Nakashima M. Seismic damage detection of a full-scale shaking table test structure. *Journal of Structural Engineering* (ASCE), 2011;137(1):14-21. https://doi.org/10.1061/(ASCE)ST.1943-541X.0000278.

44) Huang SK, Chao SH, Huang JY, et al. Estimation of story drift directly from acceleration records for post-earthquake safety evaluations of buildings. *Earthquake Engineering and Structural Dynamics*, 2021; 50(11):3064-3082. https://doi.org/10.1002/eqe.3500